



OPEN ACCESS

EDITED BY

Congzheng Han,
University of Chinese Academy of
Sciences, China

REVIEWED BY

Sooyoul Kim,
Kumamoto University, Japan
Faizal Ade Rahmahuddin Abdullah,
Bandung Institute of Technology,
Indonesia

*CORRESPONDENCE

Quan Jin

✉ jinq@hntou.edu.cn

Feng Hua

✉ huaf@stu.edu.cn

RECEIVED 26 October 2025

REVISED 25 January 2026

ACCEPTED 05 March 2026

PUBLISHED 23 March 2026

CITATION

Fang C, Jiang L, Wang Z, Jin Q, Jiang X
and Hua F (2026) WaveUformer:
a bias correction model for
GWSM4C Wave Forecasting.
Front. Mar. Sci. 13:1732870.
doi: 10.3389/fmars.2026.1732870

COPYRIGHT

© 2026 Fang, Jiang, Wang, Jin, Jiang and
Hua. This is an open-access article
distributed under the terms of the
[Creative Commons Attribution License
\(CC BY\)](https://creativecommons.org/licenses/by/4.0/). The use, distribution or
reproduction in other forums is
permitted, provided the original
author(s) and the copyright owner(s) are
credited and that the original publication
in this journal is cited, in accordance
with accepted academic practice. No
use, distribution or reproduction is
permitted which does not comply with
these terms.

WaveUformer: a bias correction model for GWSM4C Wave Forecasting

Can Fang¹, Longyu Jiang², Zeyu Wang³, Quan Jin^{4*},
Xingjie Jiang⁵ and Feng Hua^{1*}

¹Guangdong Provincial Key Laboratory of Marine Disaster Prediction and Prevention, Shantou University, Shantou, China, ²Institute of Physical Oceanography and Remote Sensing, Ocean College, Zhejiang University, Zhoushan, China, ³Ningbo Marine Center, Ministry of Natural Resources, Ningbo, Zhejiang, China, ⁴College of Marine Science and Technology, Hainan Tropical Ocean University, Sanya, China, ⁵First Institute of Oceanography and Key Laboratory of Marine Science and Numerical Modeling, Ministry of Natural Resources, Qingdao, China

Artificial intelligence (AI) models are being progressively applied to the field of wave forecasting. However, in operational forecast scenarios, these data-driven models exhibit error characteristics different from those of numerical models due to factors such as uncertainties in the driving wind fields. Traditional correction methods have limited capability to correct these data-driven biases, particularly for medium- to long-range forecasts and extreme sea states. To address this issue, this study proposes a deep learning-based post-processing correction model, WaveUformer, specifically designed to correct the forecast results of the AI wave model Global Wave Surrogate Model for Climate simulation (GWSM4C). The model synergistically processes driving wind field data and forecast wave field data, and integrates an adaptive correction mechanism based on forecast lead time with an efficient spatiotemporal attention network to effectively capture the dynamic evolution patterns of errors. Evaluation based on the full-year test data of 2023 shows that WaveUformer reduces the annual mean root mean square error of 24-240-hour significant wave height forecasts from 0.57 m to 0.39 m, achieving an overall relative improvement of 31%. In the case analysis of Typhoon, the model successfully corrected the underestimation bias of extreme conditions and accurately reproduced the spatial structure of high-wave areas. The results demonstrate that WaveUformer can reduce the forecast errors of AI models, improving their forecast accuracy and reliability.

KEYWORDS

bias correction, deep learning, GWSM4C, significant wave height, wave forecasting

1 Introduction

Ocean waves are a critical component of the marine environment, directly influencing the safety of marine engineering (Chen et al., 2023; De Girolamo et al., 2017), vessel navigation (Breunung and Balachandran, 2023; Chen et al., 2013), offshore energy development (Gonzalez et al., 2024; Ibarra-Berastegui et al., 2023), and maritime hazard warning (Valchev et al., 2018). With the continuous expansion of the global marine economy and the increasing frequency of extreme weather events, the demand for high-precision, all-weather, and long-lead-time wave forecasting has become increasingly urgent. Contemporary wave forecasting primarily relies on third-generation numerical wave models

(NWMs), such as MASNUM, WAVEWATCH III (WW III), and SWAN (Booij et al., 1999; Tolman, 1991; Yang et al., 2005), which simulate wave propagation and evolution by solving mathematical equations. However, NWMs face inherent technical bottlenecks: high-resolution simulations are computationally expensive (Ikuyajolu et al., 2023), mathematical descriptions of complex physical processes introduce approximation errors, initial conditions impose strict quality requirements, and systematic errors accumulate and propagate during long-term integrations (Li and Zhang, 2020), collectively leading to systematic biases between forecast outputs and observations. Consequently, bias correction has become an essential post-processing technique to improve forecast accuracy and enhance its operational value (Lemos et al., 2020). Early statistical correction methods, based on linear system theory such as bias subtraction, regression analysis, and quantile mapping, showed some effectiveness in addressing simple linear biases. Lemos et al. (2020) noted that when evaluating correction methods for global wave climate projections, simple mean adjustments offer limited improvement for extreme wave events, whereas quantile-based methods can better handle the entire forecast distribution. A systematic evaluation by Parker and Hill (2017) found that bivariate methods correcting both wave height and period outperformed univariate approaches, yet traditional statistical methods generally assume stable and linear error distributions, which limits their ability to capture the complex nonlinear dynamics of wave systems.

With the advancement of machine learning, deep learning-based correction methods can capture nonlinear features and have demonstrated stronger adaptability in addressing complex error patterns. Researchers have utilized Long Short-Term Memory (LSTM) networks (Hochreiter and Schmidhuber, 1997) and other models to learn and rectify the forecast results of NWMs. Londhe et al. (2016) constructed a hybrid model coupling an NWM with a neural network that predicts numerical model errors to improve 24-hour significant wave height (SWH) forecasts for four sites along the Indian coast. Da Silva et al. (2025) employed LSTM to correct WW III model SWH forecasts at three stations off the coast of Brazil, using European Centre for Medium-Range Weather Forecasts Re analysis v5 (ERA5) data and buoy observations for training. Results showed that the approach outperformed linear regression across different regions, with mean absolute error (MAE) and root mean square error (RMSE) reduced by 28%-43% and 27%-38%, respectively. To address the sample imbalance between low and high sea states, Liao et al. (2024) constructed a dual-module LSTM model, which reduced the RMSE and MAE of 24-hour SWH forecasts by 52.9% and 65.5%, respectively. In the case of Super Typhoon Rai, the model reduced RMSE by 62.8%, significantly enhancing correction performance under extreme sea conditions. Zhou et al. (2024) used the LightGBM model to learn historical error sequences and perform point-wise correction on global SWH forecasts from the European Centre for Medium-Range Weather Forecasts Integrated Forecasting System (ECMWF-IFS), reducing the RMSE of medium- to long-range forecasts by 10-20%. Correction methods have progressively expanded from single-point to two-dimensional forecast fields. Sun et al. (2022) proposed the BU-Net model, which fuses wind and wave

information to correct the SWH fields of the WW III model, lowering the RMSE of 24-72-hour forecasts by 30%-40%. Kang et al. (2024) developed a Transformer-based 2D-Geoformer to correct the error fields of NWM SWH forecasts in the Northwest Pacific, reducing RMSE by 31.7%-43.2% within a 72-hour forecast window, with particularly significant correction effects for forecast fields with large initial errors. Cao et al. (2025) introduced the TransUNet model, which integrates a Transformer into a U-Net architecture to correct ECMWF-IFS data, reducing the 24-hour forecast RMSE by over 21.55%. To meet operational demands, Zhang et al. (2024) developed a real-time rolling correction scheme for 0-240-hour SWH forecasts in the Northwest Pacific using a TrajGRU network, with a pixel-level loss function designed to focus on regions with large deviation, reducing the mean absolute error of 0-240-hour SWH forecasts in the Northwest Pacific by 12.97-46.24%.

Currently, AI forecasting is undergoing rapid development. With ECMWF deploying the Artificial Intelligence Forecasting System (AIFS) into operational use, forecasting technology is experiencing a critical transition from numerical models to AI models (Lang et al., 2024). In recent years, AI wave forecasting models represented by GWSM4C (Jin et al., 2024; Jiang et al., 2024) have demonstrated performance comparable to NWMs in hindcast validations. However, as AI models transition from research to operational use, new challenges are emerging (Cui et al., 2025). In real-world forecasting scenarios, models must process dynamic marine environments and uncertain input data. Particularly when driven by wind fields from numerical weather prediction models, the mechanisms of error propagation and accumulation differ significantly from idealized hindcast settings (Ben-Bouallegue et al., 2024). Therefore, AI models still produce errors in practical forecasts, and their error characteristics are fundamentally different from NWMs. The errors in NWMs primarily originate from approximation errors in the mathematical representation of physical processes, discretization errors, and errors in boundary condition handling, manifesting as relatively regular, systematic biases. In contrast, AI model errors are predominantly data-driven, characterized by statistical biases, generalization errors, and high sensitivity to input data quality, exhibiting complex nonlinear error patterns (McGovern et al., 2024).

Against this backdrop, developing specialized post-processing techniques for AI wave forecasting models has become a critical and pressing issue to be solved. The existing bias correction methods are primarily designed for the physics-based error characteristics of numerical models, making it difficult to effectively address the unique error patterns of AI wave models. Compared to the post-processing of numerical models, research on post-processing corrections specifically for the SWH forecasts from AI models is relatively scarce (Haupt et al., 2021).

The existing methodological framework has clear limitations. Current correction techniques, primarily designed for the error characteristics of numerical models, are ill-suited to address the unique data-driven biases and generalization errors of AI models. This issue is particularly pronounced in medium- to long-range forecasting, as most studies are confined to short-term corrections within 72 hours, neglecting improvements in longer-range forecasts

that are vital for marine engineering and shipping planning (Zhou et al., 2024). In terms of temporal modeling of correction strategies, current methods often employ a static, time-step-independent approach, failing to capture the dynamic propagation patterns of errors evolving with lead time. Critically, these approaches typically treat SWH forecasting as a univariate problem, overlooking the relationship between the wind field and the wave field. However, SWH forecast errors largely originate from the propagation of uncertainty in the input wind fields. As the fundamental driver of wave generation and propagation, the accuracy of wind forecasts directly determines the accuracy of SWH predictions (Pizzo et al., 2021; Wang and Jiang, 2024). Especially under extreme weather conditions, relying solely on historical SWH data for correction is often insufficient to capture the forecast biases induced by changes in the wind fields (Song et al., 2022). Therefore, synergistically considering wind and wave information during the correction process is crucial for accurately rectifying the systematic biases in AI model SWH forecasts.

To address the aforementioned issues, this paper proposes a novel post-processing correction technique, the WaveUformer model, specifically designed to accurately correct the SWH forecast error characteristics of AI models such as GWSM4C, to overcome the limitations of traditional correction methods in addressing the error characteristics of AI models. The remainder of this paper is organized as follows: Section 2 describes the data sources and the design of the WaveUformer correction model; Section 3 provides a comprehensive analysis of the GWSM4C forecast results and the correction results; and Section 4 summarizes the research findings and outlines future directions.

2 Data and methods

2.1 Data sources

The construction and validation of the correction model in this study utilized wind field forecast data, SWH forecast data, and reanalysis data. All data conformed to a unified spatial configuration with a spatial resolution of $0.5^\circ \times 0.5^\circ$ and covering the global ocean between 70°S and 70°N , and a temporal resolution of 6 hours.

The wind forecast data used by the model was sourced from the ECMWF-IFS. This forecasting system was initialized twice daily at 00:00 and 12:00 Coordinated Universal Time (UTC), providing a 240-hour forecast sequence, with each forecast file containing 41 time steps at 6-hour intervals. The data includes the zonal (U) and meridional (V) components of the 10-meter wind field; to more directly represent the impact of wind speed on wave height, U and V were combined into wind speed (W) using Equation 1:

$$W = \sqrt{U^2 + V^2} \quad (1)$$

The SWH forecast data was generated by the GWSM4C model, which was driven by the aforementioned ECMWF-IFS wind forecasts. The initialization times (00:00 and 12:00 UTC daily), forecast lead time (240 hours), and time step (6 hours) were kept

strictly consistent with the driving wind fields. The ground truth benchmark for model supervision and performance evaluation is the SWH product from the ERA5 dataset.

2.2 Dataset

To effectively capture the dynamic evolution of errors with forecast lead time, time-series samples were constructed using a “sliding window” approach. Specifically, for the 41 time steps in each forecast file, sliding sampling was performed with a stride of 6 hours and a window length of 5 consecutive time steps (30-hour time span). This means that for a target correction time t , the information from the current time and the four preceding time steps ($t-24$, $t-18$, $t-12$, $t-6$, t) constitutes a single sample, and each forecast file could generate 37 valid training samples.

Each constructed sample consists of multi-dimensional inputs and a supervision target. The model inputs are composed of three parts: (1) the sequence of ECMWF-IFS forecast wind fields within the 5-step window; (2) the sequence of GWSM4C SWH forecasts within the same window; (3) a lead time identifier, which specifies the target time t to be corrected for the current sample. The supervision target is defined as the ground truth SWH data from ERA5 corresponding to the final time step (t) of the window.

Based on the method described above, a wave forecast correction dataset spanning the years 2020–2023 was constructed. Data from 2020–2022 were allocated to the training set, while data from 2023 served as an independent test set. The training set comprised approximately 2,190 forecast files, totaling about 81,030 training samples; the test set contained around 730 forecast files, with about 27,010 test samples.

In this way, the correction task can be formulated as a mapping problem from multi-step forecast information to single-step true state, and the model learns and leverages the temporal evolution patterns of errors for accurate correction.

2.3 WaveUformer model

WaveUformer is a wave forecast correction model improved from the Uformer framework (Wang et al., 2022), specifically for correcting the error characteristics of AI wave forecasting models. The model employs a U-Net encoder-decoder architecture as its main framework to achieve an end-to-end correction process, as illustrated in Figure 1a.

2.3.1 Model architecture

The model’s inputs include the ECMWF-IFS wind field forecast sequence W_{t_k} and the GWSM4C SWH forecast sequence H_{t_k} for 5 consecutive time steps ($t-24$, $t-18$, $t-12$, $t-6$, t), combined with the current forecast lead time τ . The objective is to generate the corrected SWH result $H_{corrected}$ at the target time step t_0 . This process can be formulated as Equation 2:

$$H_{corrected} = f(W_{t_k}, H_{t_k}, \tau; \theta), k = -4, -3, -2, -1, 0 \quad (2)$$

where f represents the WaveUformer model and θ denotes its learnable parameters.

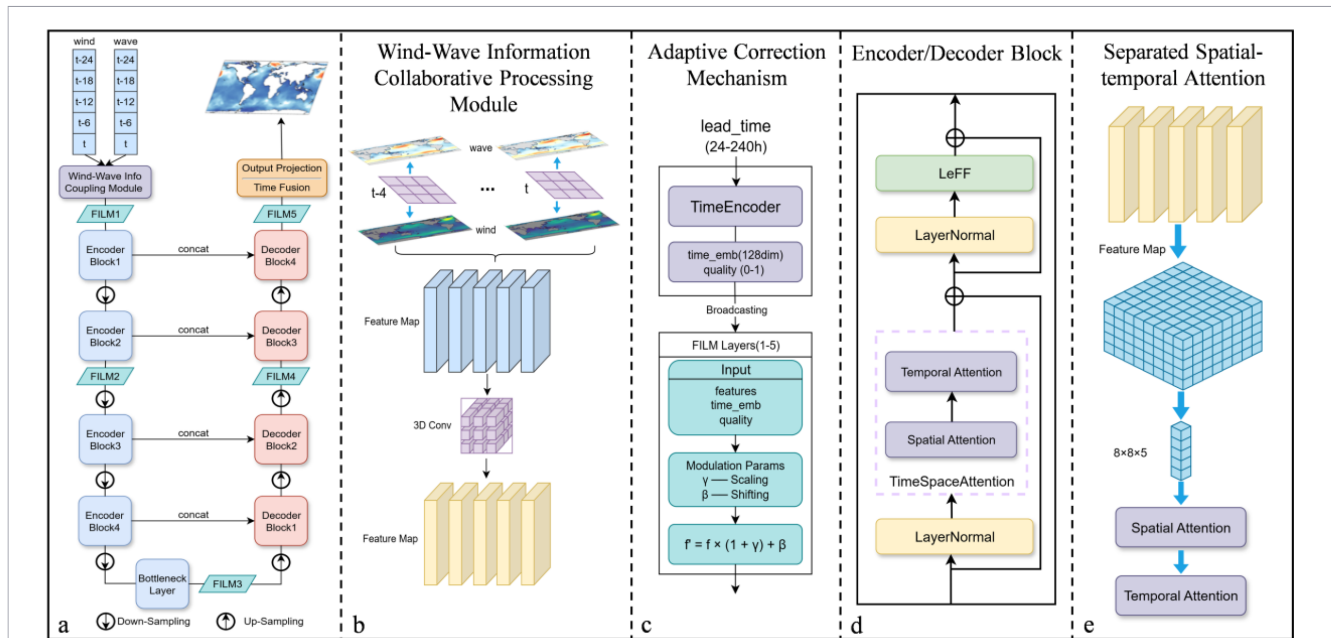


FIGURE 1 WaveUformer model architecture. (a) Main encoder-decoder framework of the model. (b) Wind-Wave Information Synergistic Processing Module. (c) Adaptive Correction Mechanism. (d) Basic structure of encoder/decoder block. (e) Attention Mechanism Module.

During the model’s forward propagation, the input wind fields and SWH data are processed simultaneously, as shown in Figure 1b. For the input 5-time-step data, each time step contains two channels: wind and SWH, and the spatial correlation between them is learned through convolutional operations. Subsequently, a three-dimensional convolution processes the 5-step sequence information to establish temporal dependencies. After this processing, the multi-step wind and SWH information is transformed into a unified spatiotemporal feature representation. Then, the adaptive correction mechanism generates temporal embeddings based on the forecast lead time and implements lead-time-aware feature modulation through Feature-wise Linear Modulation (FiLM) modulators distributed at five key locations in the model (FiLM1-5), as shown in Figure 1c. The encoder stage extracts error features at different scales through progressive downsampling, while the decoder stage combines skip connections to gradually restore spatial resolution. Within each Transformer block, as shown in Figure 1e, the spatiotemporal attention mechanism models long-range spatiotemporal dependencies while maintaining computational efficiency through separate processing of windowed spatial attention and time-series attention. Finally, a temporal fusion module aggregates the feature information from multiple time steps into a single-moment representation to directly generate the corrected SWH forecast field.

2.3.2 Lead time information encoding and adaptive correction

The forecast error of GWSM4C exhibits a nonlinear growth trend as the lead time extends (Figure 2a). This lead-time-dependent error evolution requires the correction model to dynamically adjust its correction strength according to different forecast lead times. WaveUformer addresses this issue through an

adaptive correction mechanism with lead time information encoding, which is composed of a lead time encoder and multi-level FiLM modulators working in concert. The lead time encoding module processes lead time information through a TimeEncoder function, which employs a three-layer fully connected network (32, 64, and 128 dimensions) to progressively expand the feature dimensions. This ultimately generates a 128-dimensional lead time feature embedding, $E_{temporal}$, for feature modulation, and a forecast quality assessment value, $q_{pred} \in [0, 1]$, to adjust the correction strength.

The WaveUformer model incorporates FiLM modulation at five key locations, performing adaptive scaling and shifting adjustments on features to achieve differentiated corrections at different levels (Perez et al., 2018). Each FiLM modulator has an adaptive strength control function. The modulation strength is calculated by integrating both lead time information and forecast quality, as shown in Equation 3:

$$s = \sigma(\text{MLP}_{strength}(E_{temporal})) \times (1.1 - q_{pred} + 0.1) \quad (3)$$

where σ is the Sigmoid activation function. The coefficients 1.1 and 0.1 ensure that the modulation strength remains positive and is negatively correlated with the forecast quality, meaning that lower forecast quality results in a greater correction strength. The modulation parameters are generated by independent parameter-generation networks. The scaling γ and shifting β parameters are calculated as shown in Equations 4 and 5:

$$\gamma = \tanh(\text{MLP}_{\gamma}(E_{temporal})) \odot s \quad (4)$$

$$\beta = \tanh(\text{MLP}_{\beta}(E_{temporal})) \odot s \quad (5)$$

where MLP_{γ} and MLP_{β} are the generation networks for the scaling and shifting parameters, respectively, \tanh is the hyperbolic

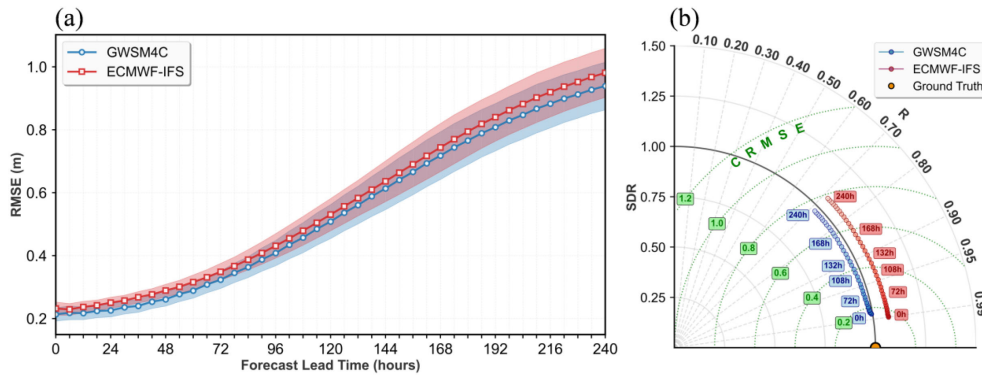


FIGURE 2 Performance comparison of 2023 SWH forecasts between GWSM4C and ECMWF-IFS. **(a)** Annual mean RMSE variation curve with forecast lead time. Blue line represents GWSM4C, red line represents ECMWF-IFS, shaded areas indicate ± 1 standard deviation range. **(b)** Taylor diagram showing R (gray arcs), SDR (radial distance), and CRMSE (green arcs). Blue line represents GWSM4C, red line represents ECMWF-IFS, numeric labels represent different forecast lead times (hours).

tangent activation function, and \odot denotes element-wise multiplication. The final feature modulation operation is defined as Equation 6:

$$F_{modulated} = F \odot (1 + \gamma) + \beta \tag{6}$$

where F is the input feature and $F_{modulated}$ is the modulated feature.

Through this adaptive correction mechanism with lead time information encoding, WaveUformer can effectively address the issue of dynamically changing errors with lead time in AI model SWH forecasts, providing targeted correction strategies for different forecast lead times.

2.3.3 Efficient spatiotemporal attention

For global-scale wave forecast data, standard global attention mechanisms are difficult to apply directly. WaveUformer employs a separated spatiotemporal attention mechanism, which processes feature learning in the temporal and spatial dimensions separately. This approach enhances computational efficiency while preserving the ability to model long-range dependencies (Tan et al., 2023; Wang et al., 2024).

Spatial attention adopts a local window strategy to reduce computational complexity. The input feature map is partitioned into non-overlapping 8×8 windows, and self-attention is computed independently within each window. When the feature map size cannot be evenly divided by the window size, a padding strategy is adopted to ensure complete coverage. Within each window, a standard self-attention mechanism is applied, and relative position encoding is added, as expressed in Equation 7:

$$\text{Attn}_i = \text{softmax} \left(\frac{Q_i K_i^T}{\sqrt{d_k}} + B_{rel} \right) V_i \tag{7}$$

where Q_i, K_i, V_i are the query, key, and value matrices of the i -th window, B_{rel} is the relative position bias matrix, and d_k is the dimension of each attention head.

After processing in the spatial dimension, temporal attention models the evolutionary relationship of the time series independently at each spatial location (i, j) . For the 5-step feature sequence at each spatial location, the temporal attention is computed as Equation 8:

$$\text{TemporalAttn}_{i,j} = \text{softmax} \left(\frac{Q_{i,j} K_{i,j}^T}{\sqrt{d_k}} \right) V_{i,j} \tag{8}$$

This design enables the model to learn the intrinsic evolutionary patterns of time series at each spatial location, capturing the continuity and change trends of SWH in the temporal dimension. Since the number of time steps is relatively small, the computational cost of temporal attention remains within an acceptable range.

2.3.4 Training strategy and optimization

The model was trained using the Charbonnier loss function (Charbonnier et al., 1997), as defined in Equation 9:

$$\mathcal{L}_{Char} = \frac{1}{N} \sum_{i=1}^N \sqrt{(\hat{H}_i - H_i^{ERA5})^2 + \epsilon^2} \tag{9}$$

where $\epsilon = 10^{-6}$ is a smoothing parameter. Compared to the standard L2 loss, the Charbonnier loss is more sensitive to small errors while being more robust to outliers. This is particularly important for handling subtle error patterns in wave forecasting (Lai et al., 2017).

Training adopted the AdamW optimizer combined with cosine annealing learning rate scheduling. It was also equipped with an early stopping mechanism based on validation loss to prevent overfitting during training.

This comprehensive framework enables WaveUformer to effectively learn and correct the complex error patterns inherent in AI wave forecasting models while maintaining computational efficiency.

3 Results

3.1 Evaluation metrics

To evaluate the performance of the GWSM4C model's SWH forecasts and the WaveUformer correction model, this study selected the RMSE, MAE, Correlation Coefficient (R), Standard Deviation Ratio (SDR), and Centered Root Mean Square Error (CRMSE) as the primary evaluation metrics. These metrics are defined by Equations 10–14:

$$RMSE = \sqrt{\frac{1}{N} \sum_{i=1}^N (y_i - \hat{y}_i)^2} \tag{10}$$

$$MAE = \frac{1}{N} \sum_{i=1}^N |y_i - \hat{y}_i| \tag{11}$$

$$R = \frac{\sum_{i=1}^N (y_i - \bar{y})(\hat{y}_i - \bar{\hat{y}})}{\sqrt{\sum_{i=1}^N (y_i - \bar{y})^2} \sqrt{\sum_{i=1}^N (\hat{y}_i - \bar{\hat{y}})^2}} \tag{12}$$

$$SDR = \frac{\sigma_{\hat{y}}}{\sigma_y} = \frac{\sqrt{\frac{1}{N} \sum_{i=1}^N (\hat{y}_i - \bar{\hat{y}})^2}}{\sqrt{\frac{1}{N} \sum_{i=1}^N (y_i - \bar{y})^2}} \tag{13}$$

$$CRMSE = \sqrt{\frac{1}{N} \sum_{i=1}^N ((\hat{y}_i - \bar{\hat{y}}) - (y_i - \bar{y}))^2} \tag{14}$$

where N is the total number of samples, y_i is ERA5 reanalysis data, serving as the ground truth value in this study, and \hat{y}_i is the model's forecast value. \bar{y} and $\bar{\hat{y}}$ are the mean values of the ground truth and forecast data, respectively. $\sigma_{\hat{y}}$ and σ_y are the standard deviations of the forecast and ground truth data, respectively.

3.2 GWSM4C forecast performance evaluation

To establish a benchmark for the subsequent correction work, this section compares its 2023 forecast results with those of the operational ECMWF-IFS model, using ERA5 as the ground truth reference. Figure 2 presents a comparison of SWH forecast performance between GWSM4C and ECMWF-IFS for 2023. As shown in Figure 2a, the annual mean RMSE of the GWSM4C 0-240-hour SWH forecast was 0.53 m, outperforming the ECMWF-IFS value of 0.56 m. Throughout the entire 0-240-hour forecast range, the error growth curve for GWSM4C consistently remained below that of ECMWF-IFS and exhibited a more gradual rate of increase, demonstrating high stability. The Taylor diagram in Figure 2b further reveals the distinct error characteristics of the two models. In terms of correlation, GWSM4C and ECMWF-IFS performed comparably, with the difference in correlation coefficients remaining within 0.003 across all lead times; the correlation coefficient decayed from 0.99 at the initial time to 0.72 at 240 hours. However, the two models exhibited a fundamental difference in forecast amplitude control. ECMWF-IFS showed a systematic overestimation across all 41 forecast time steps, with its

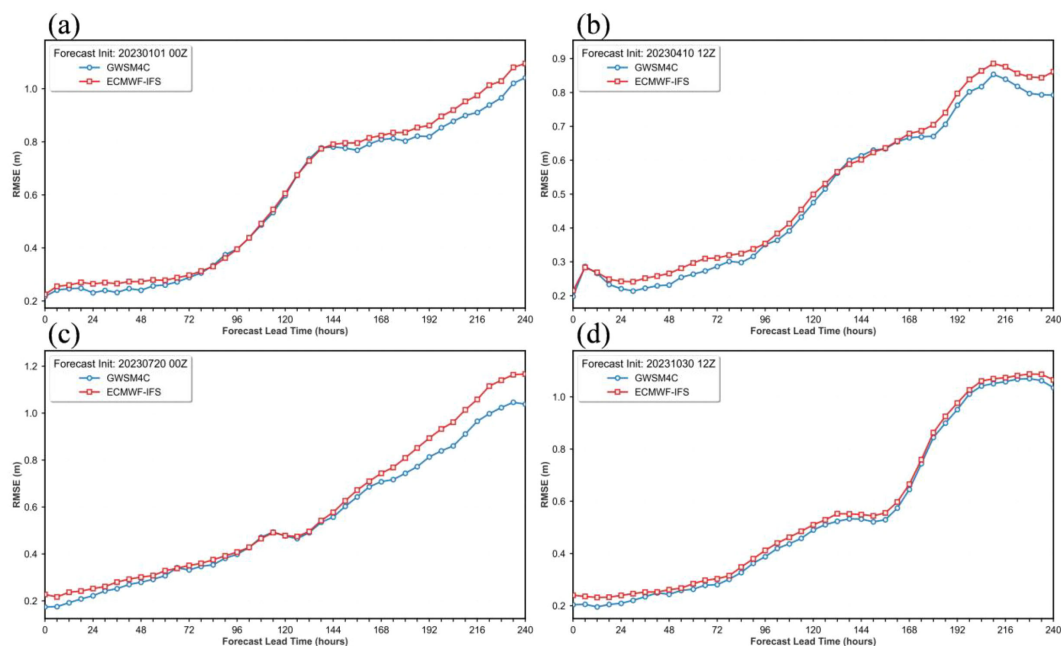


FIGURE 3 Variation of RMSE with forecast lead time for GWSM4C and ECMWF-IFS forecast cases in different seasons of 2023. The forecast initialization times in the figure are: (a) 00:00 UTC on Jan 1, 2023 (Winter); (b) 12:00 UTC on Apr 10, 2023 (Spring); (c) 00:00 UTC on Jul 20, 2023 (Summer); and (d) 12:00 UTC on Oct 30, 2023 (Autumn). Blue and red lines represent GWSM4C and ECMWF-IFS forecast results.

standard deviation ratio consistently exceeding 1.0 and an average bias of 0.07. The standard deviation ratio of GWSM4C was close to 1.0, with an average bias of only 0.02.

Figure 3 shows a comparison of forecast cases from four seasons. Across all seasonal cases, the trend of RMSE growth with forecast lead time for GWSM4C was highly consistent with that of ECMWF-IFS. In the spring case (Figure 3b), both models had the lowest overall errors, with the advantage of GWSM4C gradually emerging in medium- to long-range forecasts after 120 hours. In the summer case (Figure 3c), both models showed a linear error growth trend, and sea states were relatively calm. The changes of the two models were most similar in the autumn case (Figure 3d). The seasonal case analysis demonstrated the adaptability and robustness of GWSM4C under different sea conditions.

The comprehensive analysis fully validated the rationality and advantages of GWSM4C as a baseline SWH forecasting model. While maintaining forecast accuracy comparable to numerical models, GWSM4C demonstrated superior error control and smaller systematic bias, providing high-quality baseline forecast data for subsequent correction work.

3.3 Overall correction performance evaluation of WaveUformer

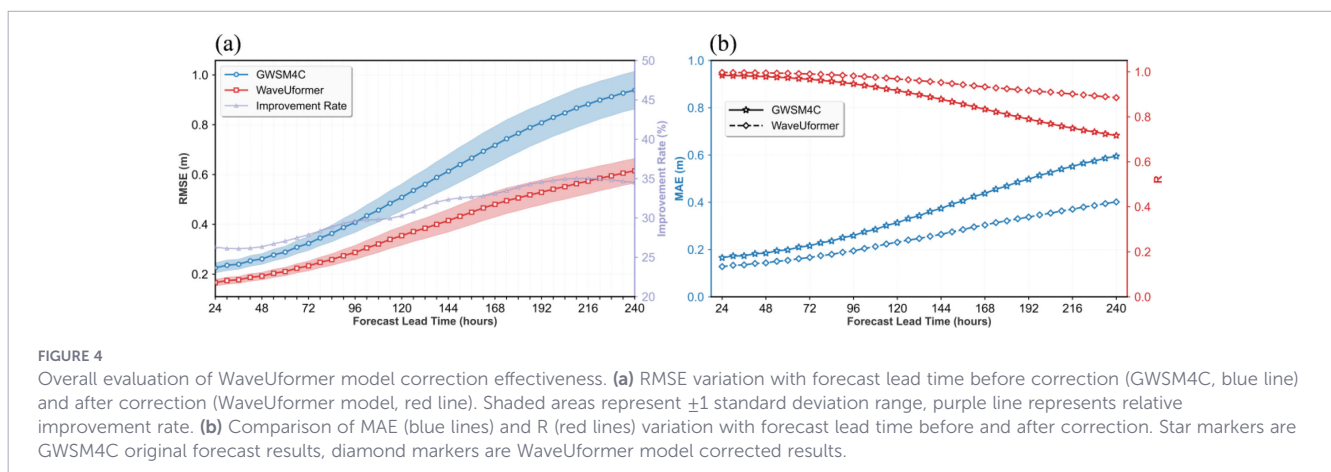
Figure 4 shows the correction effectiveness on the full-year 2023 test dataset. As shown in Figure 4a, the annual mean RMSE of the 24–240-hour SWH forecast decreased from the original 0.57 m to 0.39 m after correction, achieving an overall relative improvement of 31%. In terms of the trend of error growth with forecast lead time, the RMSE of GWSM4C SWH forecast results increased from 0.23 m at 24 hours to 0.94 m at 240 hours, while the corrected RMSE increased from 0.17 m at 24 hours to 0.62 m at 240 hours, curbing the trend of error growth with lead time. The shaded areas in the figure represent the ± 1 standard deviation range. The error dispersion before and after correction gradually increased with forecast lead time, but the standard deviation after correction was smaller than before. This indicates that WaveUformer not only reduced the mean error but also lowered the error dispersion and enhanced forecast stability. Across all 37 forecast time steps, the model's improvement rate ranged from 26% to 34%, and the improvement effect also strengthened as the forecast lead time extended.

Figure 4b presents the results for MAE and R. The average MAE of the 24–240-hour SWH forecast decreased from 0.36 m to 0.25 m after correction. The improvement in MAE also increased with lead time, rising from 24% at 24 hours to 33% at 216 hours. Meanwhile, the average R of the corrected 24–240-hour SWH forecast increased from 0.88 to 0.94, indicating that the corrected forecast results had stronger consistency with the actual spatiotemporal distribution.

3.4 Spatiotemporal distribution of correction effectiveness

Figure 5 shows the spatial distribution characteristics of RMSE reduction after correction at different forecast lead times in global ocean areas. Overall, WaveUformer effectively reduced forecast errors across most of the global ocean. The most significant improvements occurred in high-sea-state regions such as the Southern Ocean westerlies, the central North Pacific, and the eastern North Atlantic, with the correction effect generally strengthening as the forecast lead time extended. This correction is primarily attributed to the strong wind-wave coupling in these high-energy regions, which the WaveUformer's collaborative processing module effectively captures. Furthermore, the larger absolute error amplitudes in these regions provide clearer gradient signals that are naturally prioritized by the training loss function, facilitating more effective optimization compared to regions with lower sea states. In short-range forecasts (24–72-hour), the improvement effect mainly manifested as scattered small improvements (Figures 5a–e), with relatively limited overall improvement magnitude, and a few medium- to low-latitude and nearshore areas even showed slight error increases. As the forecast lead time extended, the correction effect progressively intensified. The most pronounced improvement occurred in the long-range forecast stage (≥ 168 h), especially in the Southern Ocean and medium- to high-latitude regions of the Northern Hemisphere (Figures 5m–t).

Due to significant variations in SWH characteristics across different ocean areas, evaluating model performance only through RMSE reduction has limitations. To more objectively measure the model's improvement effect, Figure 6 shows the spatial distribution of relative RMSE reduction rate at different forecast lead times. This metric is calculated by dividing the RMSE reduction by the annual



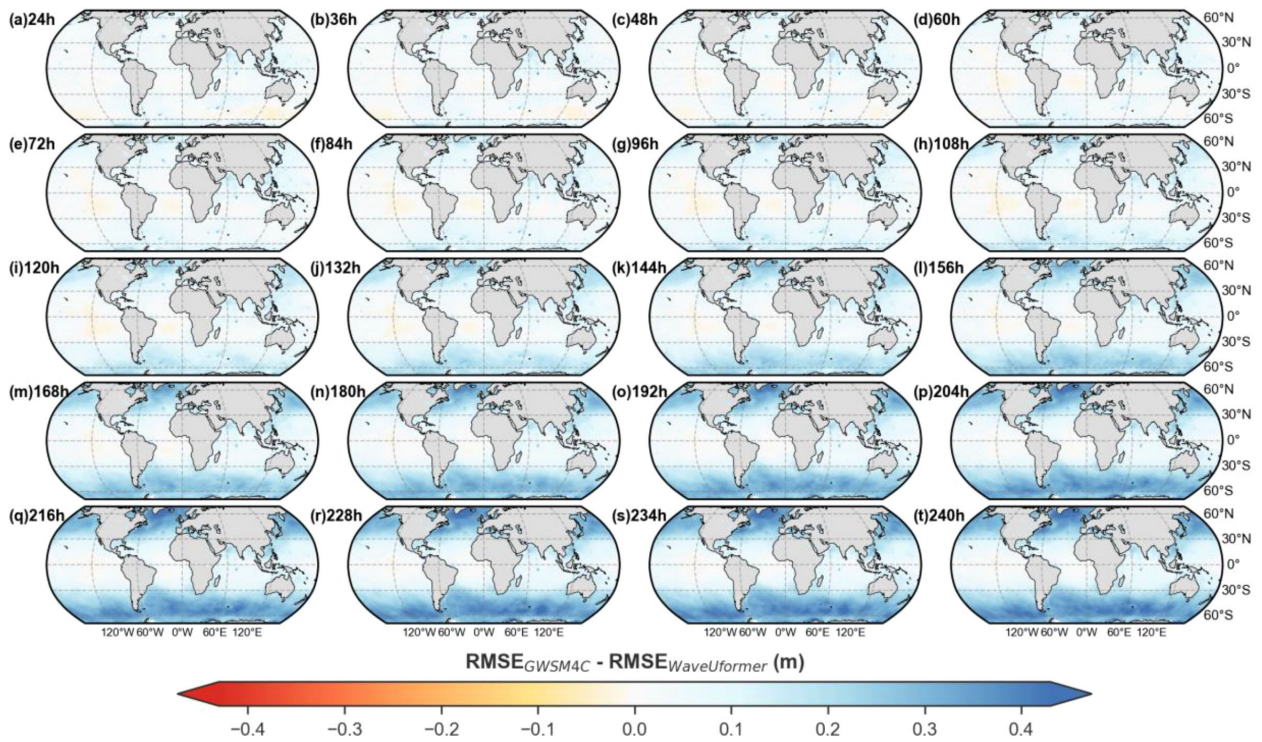


FIGURE 5
Global spatial distribution of RMSE reduction after correction. Shows the global distribution of RMSE difference before and after correction at different forecast lead times from 24h to 240h. Blue areas represent regions of RMSE decrease, and red areas represent regions of RMSE increase.

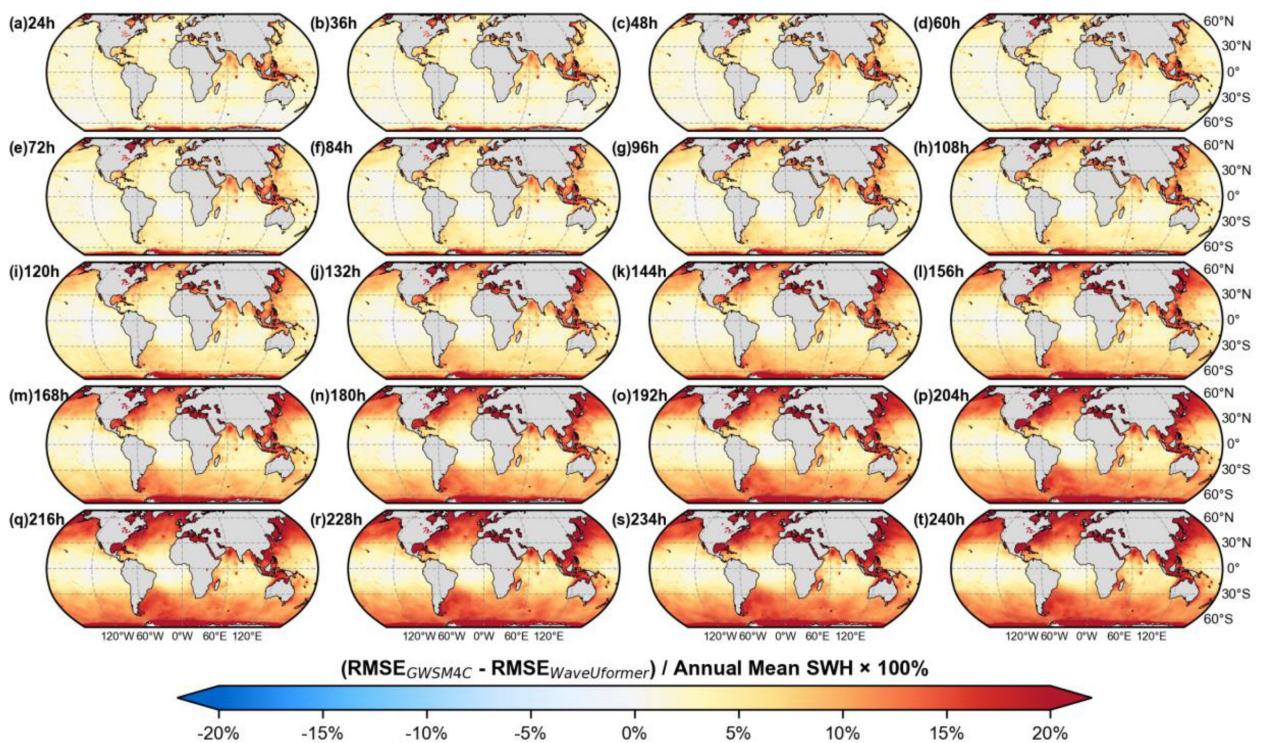


FIGURE 6
Global spatial distribution of relative RMSE reduction rate after correction. Shows the global distribution of relative RMSE reduction rate at different forecast lead times from 24h to 240h. Red areas represent regions where the relative RMSE decreased, and blue areas represent regions where it increased.

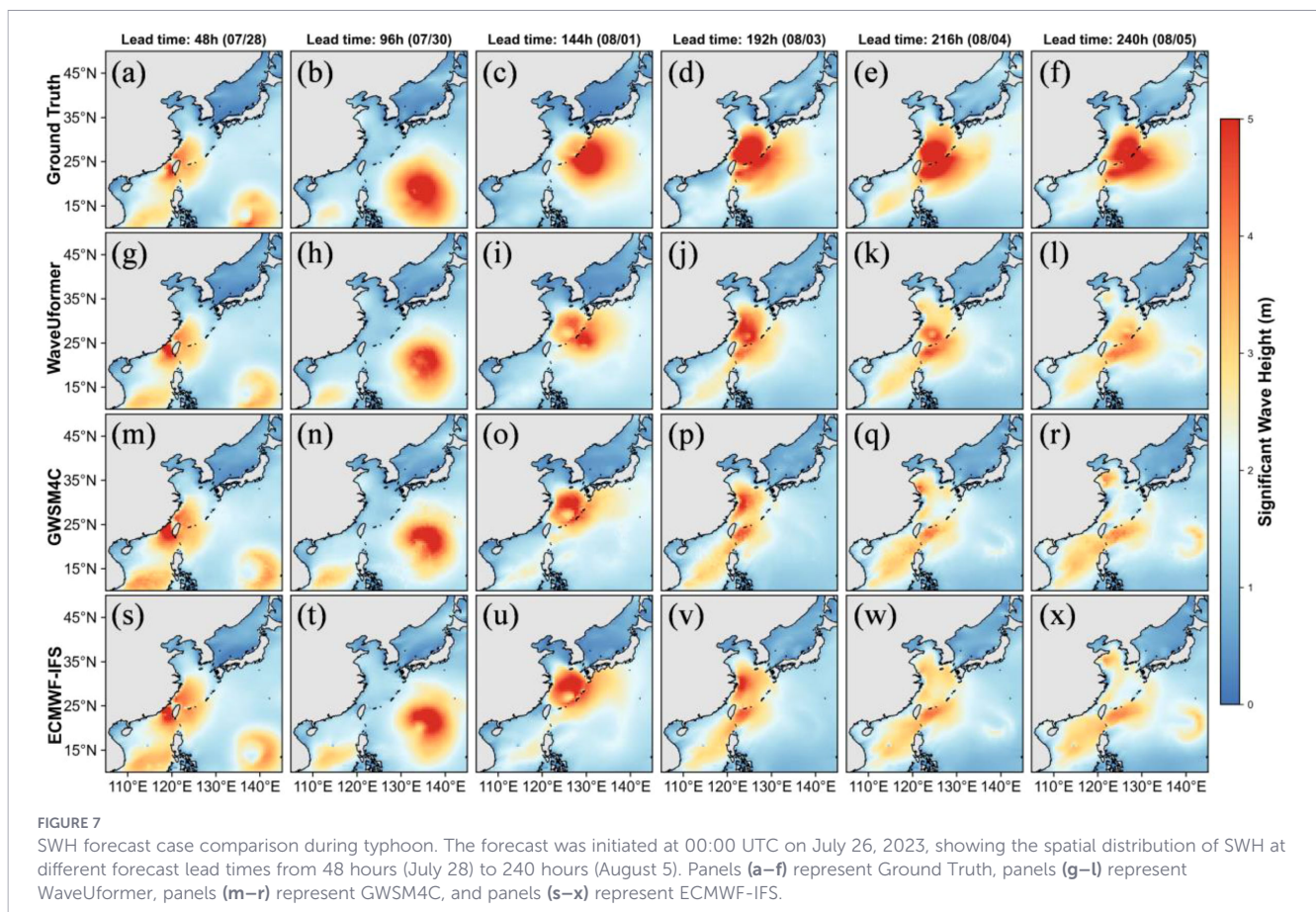
mean SWH, and its spatial distribution characteristics differed markedly from RMSE reduction. The highest relative reduction rates were found in low-latitude regions, particularly the low-latitude western Pacific, the Arabian Sea and Bay of Bengal in the northern Indian Ocean, and the equatorial eastern Pacific, where the relative RMSE reduction reached 10-15%. Although these areas had lower average wave heights and limited absolute RMSE reductions, the correction model effectively reduced their relative errors. In contrast, although the Southern Ocean westerlies had the largest RMSE reduction, due to the higher SWH in this region, the relative RMSE reduction rate was lower, approximately 5-10%. This spatial discrepancy between absolute and relative reduction patterns is primarily governed by normalization effects. In low-latitude regions characterized by small background wave heights, even minor absolute corrections translate into substantial percentage improvements. Conversely, in high-energy regions, the large mean SWH results in smaller relative reductions despite significant decreases in absolute RMSE.

3.5 Verification of correction performance under extreme sea conditions

To validate the model's performance under extreme sea conditions, this study selected a forecast from the active typhoon period in the Northwest Pacific during the summer of 2023 for analysis. The forecast was initiated at 00:00 UTC on July 26 and covered various forecast lead times from 48 to 240 hours. This forecast period encompassed the

dissipation of Super Typhoon Doksuri (formed on July 21, made landfall in Fujian on July 28) and the development and intensification of Typhoon Khanun (formed east of the Philippines on July 26). During this time, the SWH in multiple areas of the Northwest Pacific exceeded 5 meters, making it suitable for examining the correction model's ability to handle extreme sea states at medium- to long-range forecast lead times.

Figure 7 compares the SWH spatial distribution among Ground Truth, WaveUformer, GWSM4C, and ECMWF-IFS at different forecast lead times. The forecast results of GWSM4C and ECMWF-IFS showed consistency in the overall trend, both capturing the high-wave region during the typhoon period. However, compared to the Ground Truth, both forecast models exhibited significant and similar biases. At the 48- and 96-hour forecast lead times, corresponding to the landfall and dissipation of Doksuri and the initial stage of Khanun, both GWSM4C and ECMWF-IFS were able to represent the two high-wave areas off the coast of Fujian and in the eastern waters of the Philippines (Figures 7M, N, S, T). As the lead time extended to 144 and 192 hours, Khanun rapidly intensified into a super typhoon and moved northwestward. The high-wave region was concentrated in the area from northeastern Taiwan to the Ryukyu Islands. The high-wave areas forecasted by GWSM4C and ECMWF-IFS showed a noticeable positional shift and a dispersed spatial structure (Figures 7O, P, U, V). At the 216- and 240-hour lead times, the forecast errors of GWSM4C and ECMWF-IFS continued to accumulate. The position, intensity, and spatial morphology of the high-wave region deviated significantly, and the forecasted high-wave area had almost dissipated, with its spatial form becoming indistinct (Figures 7Q, R, W, X).



By comparison, the WaveUformer correction results improved these biases. As seen in Figures 7G–L, the corrected results agreed better with the Ground Truth in both SWH peak forecasting and spatial morphology representation. Within the 144- to 216-hour forecast lead times, WaveUformer accurately predicted SWH peaks exceeding 5 meters (Figures 7I–K), effectively rectifying the underestimation bias of GWSM4C. In terms of spatial morphology, its forecasted high-wave area had clear contours and concentrated range, very close to the spatial morphology of the Ground Truth. Taking the 192-hour forecast lead time as an example (Figure 7J), WaveUformer not only corrected the location and magnitude of the SWH peak, but also clearly characterized the range and shape of the high-wave area in the northeast direction of the typhoon's movement path, as well as the gradient decay from the high-wave area towards the periphery, spatial details that were not reflected in the forecasts of GWSM4C and ECMWF-IFS. At the 240-hour lead time, WaveUformer could still roughly represent the location of the SWH peak and the basic contour of the high-wave region (Figure 7L), whereas in the GWSM4C and ECMWF-IFS forecasts, the high-wave region had largely dissipated, and both failed to predict the spatial pattern accurately (Figure 7R, X). These results validated that WaveUformer can correct SWH forecast errors under extreme sea conditions. To further validate these results, quantitative comparisons for high-sea-state regions ($SWH \geq 4.0$ m) are summarized in Table 1. The statistical metrics show high consistency with the spatial patterns in Figure 7. In the short-term forecast (48 h), the WaveUformer effectively corrected the significant overestimation of GWSM4C, reducing the mean bias from 0.47 m to 0.01 m. As the lead time extended to 144–240 h, systematic underestimation persisted in both models, which is largely attributable to the intensity uncertainties inherited from the driving wind fields. Nevertheless, the WaveUformer significantly mitigated these errors by recovering the underestimated SWH magnitude. At 192 h, the correction model improved the mean bias from -2.54 m to -1.86 m and reduced the RMSE by approximately 29% (from 3.07 m to 2.18 m). Moreover, regarding the spatial structure, the WaveUformer demonstrated

superior robustness. While the R of GWSM4C dropped to 0.60 at 240 h, the WaveUformer maintained a high correlation of 0.88, indicating that the spatio-temporal attention mechanism effectively preserves the structural integrity of the typhoon wave fields even under long-term forecast horizons. It is worth noting that as a post-processing method, WaveUformer inevitably inherits spatial phase information from the driving wind fields and baseline forecasts to some extent, resulting in corrected spatial patterns that still partially resemble the baseline forecasts. Consequently, when storm-track errors dominate, correcting intensity alone is insufficient to fully eliminate displacement or structural mismatches.

4 Conclusions and outlook

This study conducted work on post-processing correction of AI wave forecasting models and proposed the WaveUformer correction method specifically for the error characteristics of AI models. A complete process from forecasting to correction was established using the GWSM4C model, validating the technical feasibility and practical effectiveness of the proposed correction method. Furthermore, after training, the GWSM4C model can be uniformly applied to both hindcasting and forecasting tasks for SWH. This approach ensures the consistency of results in different application scenarios. Compared to studies focused solely on hindcast scenarios, it expands the application boundaries of the GWSM4C model. This research has made progress in forecast data construction, correction method innovation, and application validation. The main conclusions are as follows:

- A complete wave forecast dataset was established based on the GWSM4C model. The model's annual mean RMSE of 0.53 m was superior to the 0.56 m of ECMWF-IFS, representing an overall relative error reduction of 5.3%. It maintained stable performance throughout the entire 0-240-hour forecast lead time, providing high-quality forecast data for subsequent correction work.
- The WaveUformer correction model corrects the SWH forecast error characteristics of GWSM4C. During the correction process, it synergistically processes wind and wave field information; its adaptive correction mechanism dynamically adjusts correction strategies based on forecast lead time; and its efficient spatiotemporal attention mechanism balances forecast accuracy with computational efficiency while ensuring precise capture of error evolution patterns. This effectively corrects forecast biases arising from the propagation of uncertainty in the driving wind field.
- Correction results show that the annual mean RMSE of SWH forecasts decreased from 0.57 m to 0.39 m, with an overall improvement of 31%. Within the 24-240-hour forecast lead time, the correction model improvement rate ranged from 26% to 34%. The Super Typhoon Doksuri case validated that the correction method can correct SWH forecast errors under extreme sea conditions. This improvement is critical for marine engineering,

TABLE 1 Comparison of mean bias, RMSE, and R for WaveUformer, GWSM4C, and ECMWF-IFS in high-sea-state regions ($SWH \geq 4.0$ m).

| Metric | Model | Lead time (h) | | | | | |
|------------------------------|-------------|---------------|-------|-------|-------|-------|-------|
| | | 48 | 96 | 144 | 192 | 216 | 240 |
| Mean Bias (≥ 4.0 m) | WaveUformer | 0.01 | -0.91 | -1.85 | -1.86 | -1.93 | -1.73 |
| | GWSM4C | 0.47 | -1.13 | -2.69 | -2.54 | -2.78 | -2.48 |
| | ECMWF-IFS | 0.21 | -1.12 | -2.51 | -2.39 | -2.49 | -2.35 |
| RMSE (≥ 4.0 m) | WaveUformer | 0.82 | 1.21 | 2.07 | 2.18 | 2.12 | 1.88 |
| | GWSM4C | 1.76 | 1.73 | 3.06 | 3.07 | 3.09 | 2.73 |
| | ECMWF-IFS | 1.38 | 1.17 | 2.91 | 2.91 | 2.81 | 2.61 |
| R | WaveUformer | 0.97 | 0.94 | 0.91 | 0.91 | 0.91 | 0.88 |
| | GWSM4C | 0.9 | 0.83 | 0.70 | 0.72 | 0.68 | 0.60 |
| | ECMWF-IFS | 0.93 | 0.83 | 0.68 | 0.73 | 0.74 | 0.64 |

particularly for determining design parameters and calculating structural wave loads. Thus, WaveUformer provides a more reliable basis for the safety assessment of offshore and coastal structures, ensuring sufficient safety margins during severe weather events.

Despite the progress made in AI wave forecast correction technology in this study, there are still some limitations that need further improvement in future work. The WaveUformer correction model mainly corrects the single element of SWH and has not yet been extended to other important wave parameters such as period and wave direction. This limits the completeness of the corrected results for applications sensitive to multiple parameters, like marine engineering design and wave energy assessment. Furthermore, the model currently focuses on intensity correction and partially inherits spatial positional errors from the driving wind fields, as observed in the typhoon case. Future work will consider incorporating training objectives focused on structural consistency to further enhance spatial consistency. Meanwhile, the “black box” characteristics of the correction model still persist, and its interpretability remains limited. Future research should combine methods such as Physics-Informed Neural Networks to embed fundamental laws of ocean dynamics into the correction model, enhancing model interpretability and physical consistency while improving forecast accuracy. Finally, although the correction model considers forecast lead time variations, its differential treatment of marine environmental characteristics across different seasons is still not sufficiently refined. Future work will investigate season-aware dynamic correction. One direction is to introduce a season embedding as an auxiliary input to the lead-time encoder, allowing the model to modulate correction parameters under different seasonal regimes. Alternatively, season-specific sub-models could be trained to better represent season-dependent error characteristics and improve seasonal correction accuracy.

The GWSM4C closed-loop system and its correction techniques constructed in this study provide an important practical foundation for the operational application of AI marine forecasting. With continuous technological improvement and application, AI marine forecasting will play an increasingly important role in improving forecast accuracy, expanding service domains, and optimizing operational efficiency. This will ultimately achieving comprehensive intellectualization of marine forecasting technology and providing strong support for the high-quality development of the marine economy and the modernization process of marine science.

Data availability statement

The raw data supporting the conclusions of this article will be made available by the authors, without undue reservation.

Author contributions

CF: Writing – original draft, Writing – review & editing, Formal analysis, Methodology, Software, Validation, Visualization. LJ: Writing – review & editing, Data curation, Methodology, Software, Supervision, Visualization. ZW: Data curation, Writing – review & editing. QJ: Funding acquisition, Methodology, Software, Supervision, Validation, Writing – review & editing. XJ: Writing – review & editing, Data curation. FH: Writing – review & editing, Conceptualization, Funding acquisition, Methodology, Project administration, Software, Supervision.

Funding

The author(s) declared financial support was received for this work and/or its publication. This research was funded by the Open Research Fund of Guangdong Provincial Key Laboratory of Marine Disaster Prediction and Prevention (GPKLMD2023005), the Shantou University Scientific Research Funded Project (NTF21036).

Conflict of interest

The author(s) declared that this work was conducted in the absence of any commercial or financial relationships that could be construed as a potential conflict of interest.

Generative AI statement

The author(s) declared that generative AI was not used in the creation of this manuscript.

Any alternative text (alt text) provided alongside figures in this article has been generated by Frontiers with the support of artificial intelligence and reasonable efforts have been made to ensure accuracy, including review by the authors wherever possible. If you identify any issues, please contact us.

Publisher's note

All claims expressed in this article are solely those of the authors and do not necessarily represent those of their affiliated organizations, or those of the publisher, the editors and the reviewers. Any product that may be evaluated in this article, or claim that may be made by its manufacturer, is not guaranteed or endorsed by the publisher.

References

- Ben-Bouallegue, Z., Clare, M. C. A., Magnusson, L., Gascon, E., Maier-Gerber, M., Janousek, M., et al. (2024). The rise of data-driven weather forecasting. *Bull. Am. Meteorol. Soc.* 105, E864–E883. doi: 10.1175/BAMS-D-23-0162.1
- Booij, N., Ris, R. C., and Holthuijsen, L. H. (1999). A third-generation wave model for coastal regions: 1. Model description and validation. *J. Geophys. Res. Oceans.* 104, 7649–7666. doi: 10.1029/98JC02622
- Breunung, T., and Balachandran, B. (2023). Data-driven, high resolution ocean wave forecasting and extreme wave predictions. *Ocean. Eng.* 268, 113271. doi: 10.1016/j.oceaneng.2022.113271
- Cao, Y., Zhang, S., Lv, G., Yu, M., and Ai, B. (2025). AI-based correction of wave forecasts using the transformer-enhanced UNet model. *Adv. Atmospheric. Sci.* 42, 221–231. doi: 10.1007/s00376-024-3319-3
- Charbonnier, P., Blanc-Feraud, L., Aubert, G., and Barlaud, M. (1997). Deterministic edge-preserving regularization in computed imaging. *IEEE Trans. Img. Process.* 6, 298–311. doi: 10.1109/83.551699
- Chen, J., Milne, L., Taylor, P. H., Gunawan, D., and Zhao, W. (2023). Forward prediction of surface wave elevations and motions of offshore floating structures using a data-driven model. *Ocean. Eng.* 281, 114680. doi: 10.1016/j.oceaneng.2023.114680
- Chen, C., Shiotani, S., and Sasa, K. (2013). Numerical ship navigation based on weather and ocean simulation. *Ocean. Eng.* 69, 44–53. doi: 10.1016/j.oceaneng.2013.05.019
- Cui, Y., Wu, R., Zhang, X., Zhu, Z., Liu, B., Shi, J., et al. (2025). Forecasting the eddying ocean with a deep neural network. *Nat. Commun.* 16, 2268. doi: 10.1038/s41467-025-57389-2
- Da Silva, M. B. L., Barreto, F. T. C., Costa, M. C. D. O., Da Silva Junior, C. L., and De Camargo, R. (2025). Bias correction of significant wave height with LSTM neural networks. *Ocean. Eng.* 318, 120015. doi: 10.1016/j.oceaneng.2024.120015
- De Girolamo, P., Di Risio, M., Beltrami, G. M., Bellotti, G., and Pasquali, D. (2017). The use of wave forecasts for maritime activities safety assessment. *Appl. Ocean. Res.* 62, 18–26. doi: 10.1016/j.apor.2016.11.006
- Gonzalez, N., Serna-Torre, P., Sánchez-Pérez, P. A., Davidson, R., Murray, B., Staadecker, M., et al. (2024). Offshore wind and wave energy can reduce total installed capacity required in zero-emissions grids. *Nat. Commun.* 15, 6826. doi: 10.1038/s41467-024-50040-6
- Haupt, S. E., Chapman, W., Adams, S. V., Kirkwood, C., Hosking, J. S., Robinson, N. H., et al. (2021). Towards implementing artificial intelligence post-processing in weather and climate: proposed actions from the Oxford 2019 workshop. *Philos. Trans. R. Soc. Math. Phys. Eng. Sci.* 379, 20200091. doi: 10.1098/rsta.2020.0091
- Hochreiter, S., and Schmidhuber, J. (1997). Long short-term memory. *Neural Comput.* 9, 1735–1780. doi: 10.1162/neco.1997.9.8.1735
- Ibarra-Berastegui, G., Sáenz, J., Ulazia, A., Sáenz-Aguirre, A., and Esnaola, G. (2023). CMIP6 projections for global offshore wind and wave energy production, (2015–2100). *Sci. Rep.* 13, 18046. doi: 10.1038/s41598-023-45450-3
- Ikuyajolu, O. J., Roekel, L. V., Brus, S. R., Thomas, E. E., Deng, Y., and Sreepathi, S. (2023). Porting the WAVEWATCH III (v6.07) wave action source terms to GPU. *Geosci. Model. Dev.* 16, 2515–2531. doi: 10.5194/gmd-16-1445-2023
- Jiang, L., Jin, Q., Hua, F., Jiang, X., Wang, Z., Gao, W., et al. (2024). Numerical investigation of the effective receptive field and its relationship with convolutional kernels and layers in convolutional neural network. *Front. Mar. Sci.* 11. doi: 10.3389/fmars.2024.1492572
- Jin, Q., Jiang, X., Hua, F., Yang, Y., Jiang, S., Yu, C., et al. (2024). GWSM4C: A global wave surrogate model for climate simulation based on a convolutional architecture. *Ocean. Eng.* 309, 118458. doi: 10.1016/j.oceaneng.2024.118458
- Kang, X., Song, H., Zhang, Z., Yin, X., and Gu, J. (2024). A transformer-based method for correcting significant wave height numerical forecasting errors. *Front. Mar. Sci.* 11. doi: 10.3389/fmars.2024.1374902
- Lai, W.-S., Huang, J.-B., Ahuja, N., and Yang, M.-H. (2017). “Deep laplacian pyramid networks for fast and accurate super-resolution,” in *Proceedings of the IEEE Conference on Computer Vision and Pattern Recognition (CVPR)*. (Honolulu, HI; IEEE) 5835–5843. doi: 10.1109/CVPR.2017.618
- Lang, S., Alexe, M., Chantry, M., Dramsch, J., Pinault, F., Raoult, B., et al. (2024). AIFS – ECMWF’s data-driven forecasting system. *arXiv [preprint]*. doi: 10.48550/arXiv.2406.01465
- Lemos, G., Menendez, M., Semedo, A., Camus, P., Hemer, M., Dobrynin, M., et al. (2020). On the need of bias correction methods for wave climate projections. *Glob. Planet. Change* 186, 103109. doi: 10.1016/j.gloplacha.2019.103109
- Li, J., and Zhang, S. (2020). Mitigation of model bias influences on wave data assimilation with multiple assimilation systems using WaveWatch III v5.16 and SWAN v41.20. *Geosci. Model. Dev.* 13, 1035–1054. doi: 10.5194/gmd-13-1035-2020
- Liao, J., Li, Y., Li, J., Li, S., and Peng, S. (2024). A two-module bias-correction model for sea wave hindcasting based on the long-short term memory neural network. *Ocean. Eng.* 311, 118827. doi: 10.1016/j.oceaneng.2024.118827
- Londhe, S. N., Shah, S., Dixit, P. R., Nair, T. M. B., Sirisha, P., and Jain, R. (2016). A coupled numerical and artificial neural network model for improving location specific wave forecast. *Appl. Ocean. Res.* 59, 483–491. doi: 10.1016/j.apor.2016.07.004
- McGovern, A., Bostrom, A., McGraw, M., Chase, R. J., Gagne, D. J., Ebert-Uphoff, I., et al. (2024). Identifying and categorizing bias in AI/ML for earth sciences. *Bull. Am. Meteorol. Soc.* 105, E567–E583. doi: 10.1175/BAMS-D-23-0196.1
- Parker, K., and Hill, D. F. (2017). Evaluation of bias correction methods for wave modeling output. *Ocean. Model.* 110, 52–65. doi: 10.1016/j.ocemod.2016.12.008
- Perez, E., Strub, F., De Vries, H., Dumoulin, V., and Courville, A. (2018). “FiLM: visual reasoning with a general conditioning layer,” in *Proceedings of the AAAI Conference on Artificial Intelligence*, Vol. 32 (New Orleans, LA, USA: AAAI Press). doi: 10.1609/aaai.v32i1.11671
- Pizzo, N., Deike, L., and Ayet, A. (2021). How does the wind generate waves? *Phys. Today* 74, 38–43. doi: 10.1063/PT.3.4880
- Song, T., Han, R., Meng, F., Wang, J., Wei, W., and Peng, S. (2022). A significant wave height prediction method based on deep learning combining the correlation between wind and wind waves. *Front. Mar. Sci.* 9. doi: 10.3389/fmars.2022.983007
- Sun, D., Huang, W., Luo, Y., Luo, J., Wright, J. S., Fu, H., et al. (2022). A deep learning-based bias correction method for predicting ocean surface waves in the northwest pacific ocean. *Geophys. Res. Lett.* 49, e2022GL100916. doi: 10.1029/2022GL100916
- Tan, C., Gao, Z., Wu, L., Xu, Y., Xia, J., Li, S., et al. (2023). “Temporal attention unit: towards efficient spatiotemporal predictive learning,” in *Proceedings of the IEEE/CVF Conference on Computer Vision and Pattern Recognition (CVPR)*. (Vancouver, BC, Canada: IEEE), 18770–18782. doi: 10.1109/CVPR52729.2023.01800
- Tolman, H. L. (1991). A third-generation model for wind waves on slowly varying, unsteady, and inhomogeneous depths and currents. *J. Phys. Oceanogr.* 21, 782–797. doi: 10.1175/1520-0485(1991)021<0782:ATGMFW>2.CO;2
- Valchev, N., Eftimova, P., and Andreeva, N. (2018). Implementation and validation of a multi-domain coastal hazard forecasting system in an open bay. *Coast. Eng.* 134, 212–228. doi: 10.1016/j.coastaleng.2017.08.008
- Wang, Z., Cun, X., Bao, J., Zhou, W., Liu, J., and Li, H. (2022). “Uformer: A general U-shaped transformer for image restoration,” in *Proceedings of the IEEE/CVF Conference on Computer Vision and Pattern Recognition (CVPR)*. (New Orleans, LA, USA: IEEE), 17662–17672. doi: 10.1109/CVPR52688.2022.01716
- Wang, X., and Jiang, H. (2024). Physics-guided deep learning for skillful wind-wave modeling. *Sci. Adv.* 10, eadr3559. doi: 10.1126/sciadv.adr3559
- Wang, P., Wang, K., Song, Y., and Wang, X. (2024). AutoLDT: a lightweight spatio-temporal decoupling transformer framework with AutoML method for time series classification. *Sci. Rep.* 14, 29801. doi: 10.1038/s41598-024-81000-1
- Yang, Y., Qiao, F., Zhao, W., Teng, Y., and Yuan, Y. (2005). MASNUM ocean wave numerical model in spherical coordinates and its application. *Acta Oceanol. Sin.* 27, 1–7.
- Zhang, W., Sun, Y., Wu, Y., Dong, J., Song, X., Gao, Z., et al. (2024). A deep-learning real-time bias correction method for significant wave height forecasts in the Western North Pacific. *Ocean. Model.* 187, 102289. doi: 10.1016/j.ocemod.2023.102289
- Zhou, S., Wang, J., Cao, Y., Bethel, B. J., Xie, W., Xu, G., et al. (2024). Improving the accuracy of global ECMWF wave height forecasts with machine learning. *Ocean. Model.* 192, 102450. doi: 10.1016/j.ocemod.2024.102450